Ocean circulation influences on sea surface temperature in the equatorial central Pacific

Chunzai Wang

Physical Oceanography Division, NOAA Atlantic Oceanographic and Meteorological Laboratory
Miami, Florida, USA

Robert H. Weisberg

College of Marine Science, University of South Florida, St. Petersburg, Florida, USA

Abstract. Velocity data from an array of acoustic Doppler current profilers moored about 0°, 140°W from May 1990 through June 1991 during the Tropical Instability Wave Experiment are used in conjunction with Tropical Atmosphere-Ocean array data and a blended sea surface temperature (SST) product to study the processes that control SST variations. The horizontal velocity data allow us to calculate the vertical velocity component by vertically integrating the continuity equation. Given the three-dimensional temperature flux divergence, we examine the role of the ocean circulation in SST. Upwelling and downwelling are found to be associated with cooling and warming, respectively, suggesting that a vertical velocity component of either sign affects SST. Both the temperature flux divergence and advective formulations for the ocean circulation's influence on the temperature budget show times when the ocean circulation appears to provide the primary control on SST and times when this is not the case, with the flux divergence formulation performing better than the advective formulation. Statistically, within a bandwidth encompassing the tropical instability waves and the intraseasonal variations, roughly half of the SST variation is accounted for by the ocean circulation. These results are encouraging, given that data sets with different spatial and temporal scales have been used. They suggest that future field experimentation which utilizes a flux divergence array with velocity and temperature data sampled at the same spatial and temporal scales will yield quantitatively improved results. The analyses also show that the ocean circulation, on average, provides a cooling effect requiring the net surface heat flux to be positive to maintain the mean background state. The cooling effect is mainly controlled by mean ocean circulation and temperature fields.

1. Introduction

Understanding the physical processes that control sea surface temperature (SST) variations in the tropics is a necessary step toward improving climate prediction. There have been numerous numerical models developed for studying the different processes that may be responsible for tropical SST variations on different timescales [e.g., *Koberle and Philander*, 1994]. However, observational studies in support of such models remain incomplete because of a lack of measurements for estimating all of the terms in the SST equation. In particular, with the vertical velocity component too small to measure, the upwelling and downwelling influences on SST remain ill defined. For the equatorial eastern Pacific, *Hayes et al.* [1991] assessed the importance of the various oceanic and atmospheric processes in the mixed layer temperature using observations from moorings. A single current meter mooring, however, does not allow for the estimate of the vertical velocity to assess the upwelling and downwelling processes. Also lacking vertical velocity information, *Kessler and McPhaden* [1995] adopted a parameterization for upwelling-induced SST variations at 0°, 140°W dependent upon the zonal wind stress and the thermo-

cline depth. For the equatorial Atlantic Ocean, *Weingartner and Weisberg* [1991a, 1991b] used an array of moored current meters to estimate the vertical velocity component from the horizontal divergence. The fully three-dimensional (3-D) advection was found to be important for SST as the thermocline responded to the seasonal intensification of wind stress. The vertical velocity component in the equatorial Pacific has been previously estimated using current meter measurements [e.g., *Halpern and Freitag*, 1987; *Halpern et al.*, 1989; *Bryden and Brady*, 1989], but 3-D ocean circulation influences on SST have not been fully assessed on the basis of moored measurements in the equatorial Pacific Ocean.

From May 1990 to June 1991 an array of five subsurface acoustic Doppler current profilers (ADCP) was deployed about 0°, 140°W during the Tropical Instability Wave Experiment (TIWE). This TIWE equatorial array allows us to calculate the vertical velocity component by vertically integrating the continuity equation and by using centered differences for the horizontal divergence. Therefore the TIWE data set, in conjunction with the Tropical Atmosphere-Ocean (TAO) array data [*McPhaden*, 1993] and the blended SST product [*Reynolds and Smith*, 1995], provides an opportunity to assess the 3-D ocean circulation influences on SST in the equatorial central Pacific. This study reports an observational result of the role of ocean circulation in equatorial central Pacific SST variations.
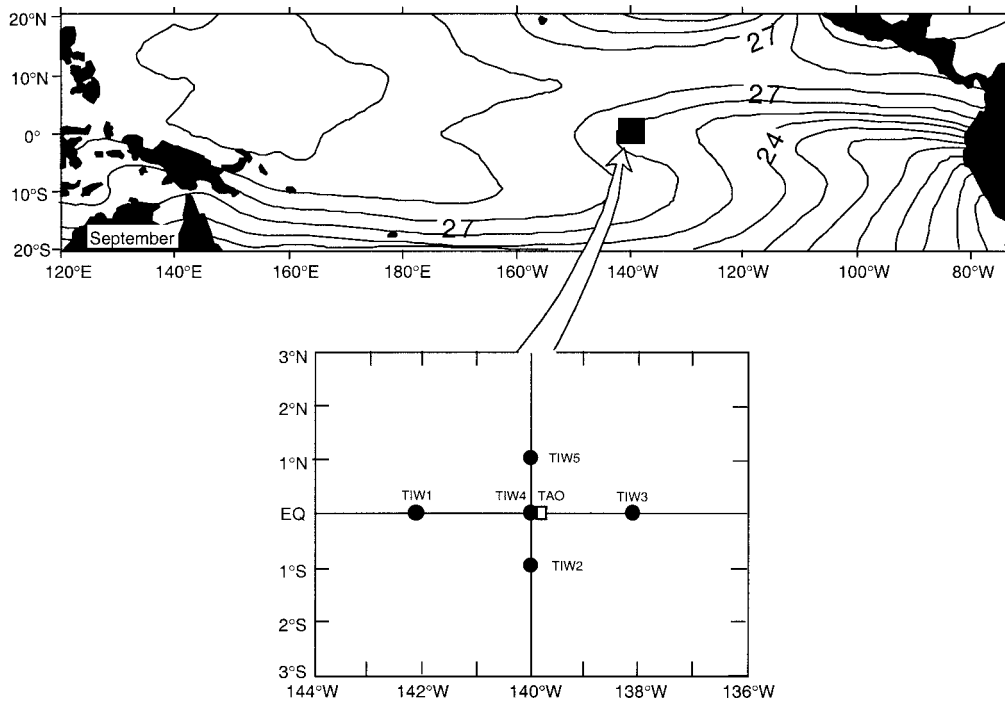
Figure 1. Location of the TIWE equatorial (circles) and TAO (open square) moorings relative to the tropical Pacific Ocean's climatological SST distribution for the month of September.

2. The Data

The TIWE moorings, designated TIW1, TIW2, TIW3, TIW4, and TIW5, were deployed in a diamond-shaped array centered upon 0°, 140°W, as shown in Figure 1. The horizontal velocity data consist of hourly samples with a 10-m vertical resolution between depths of 30 and 250 m. Estimates from 20 m to the surface are made by linear extrapolation using the 40- to 30-m shear. These hourly horizontal velocity data were averaged to daily values. In this study, the TIWE velocity data are used in conjunction with the TAO data [*McPhaden*, 1993] and the blended SST product [*Reynolds and Smith*, 1995]. Since the blended SST product is weekly, we herein focus on variabilities at frequencies lower than tropical instability wave timescales. All of the data have been low-pass filtered to remove oscillations at timescales shorter than 10 days.

The small magnitude of ocean vertical velocity makes direct observations difficult. However, the TIWE array of horizontal velocity data allows us to estimate vertical velocity through vertical integration of the continuity equation

$$\frac{\partial u}{\partial x} + \frac{\partial v}{\partial y} + \frac{\partial w}{\partial z} = 0, \tag{1}$$

where u, v, and w are the velocity components in the zonal (x), meridional (y), and vertical (z) directions, respectively. Centered differences using TIW3 and TIW1 for the zonal derivative and TIW5 and TIW2 for the meridional derivative provide the estimates of the horizontal divergence at TIW4. Equation (1) was then vertically integrated from the surface (assuming a rigid lid boundary condition: $w = 0$ at $z = 0$) to depth z to obtain w. Detailed discussions of these estimates and their errors are given by *Weisberg and Qiao* [2000]. *Qiao and Weisberg* [1995, 1997, 1998] describe the kinematics of the instability waves observed during TIWE, the dynamical balances of the upper ocean currents, and the energetic interactions between the instability waves and the currents, respectively.

Several previous studies also estimated vertical velocity by this method using moored horizontal velocity, but none with high vertical resolution or with an array that provides for centered differences. Using observations near 110°W and at different zonal separations between 140°W and 110°W, *Halpern and Freitag* [1987] and *Halpern et al.* [1989], respectively, obtained results of the vertical velocity similar to that obtained by *Bryden and Brady* [1985] in a diagnostic model using historical hydrographic data for the region 5°S–5°N, 150°W–110°W. Upwelling was found across the entire Equatorial Undercurrent (EUC), with smaller downwelling below.

The w estimate from the TIWE equatorial array is shown as a function of depth and time in Figure 2, along with the isotherms from the adjacent TAO temperature mooring (~9 km east of TIW4, as shown in Figure 1). Time series of the velocity components (u, v, and w) at 30 m depth (where the shallowest velocities are measured) at TIW4 are shown in Figure 3, along with the zonal wind stress component and SST from the adjacent TAO mooring. With the midthermocline denoted roughly by the 20°C isotherm it is noted that the vertical flow, on average, is directed upward above and downward below the midthermocline. On average, the position of maximum upwelling occurs at ~60 m depth, which corresponds to the base of the mixed layer that is located well above the EUC core at ~110 m depth.

From midsummer 1990 through midwinter 1991, when the easterly wind stress is most strongly developed, upwelling tends to be strong, SST is correspondingly cool, and the near-surface zonal flow is westward. Beginning in midwinter 1991, when the easterly wind stress relaxes, upwelling decreases, SST increases, and the near-surface zonal flow reverses to eastward. These variabilities are manifestations of the seasonal cycle in

w at 0°, 140°W (10⁻³ cm/s)

(a)

Temperature at 0°, 140°W (°C)

(b)
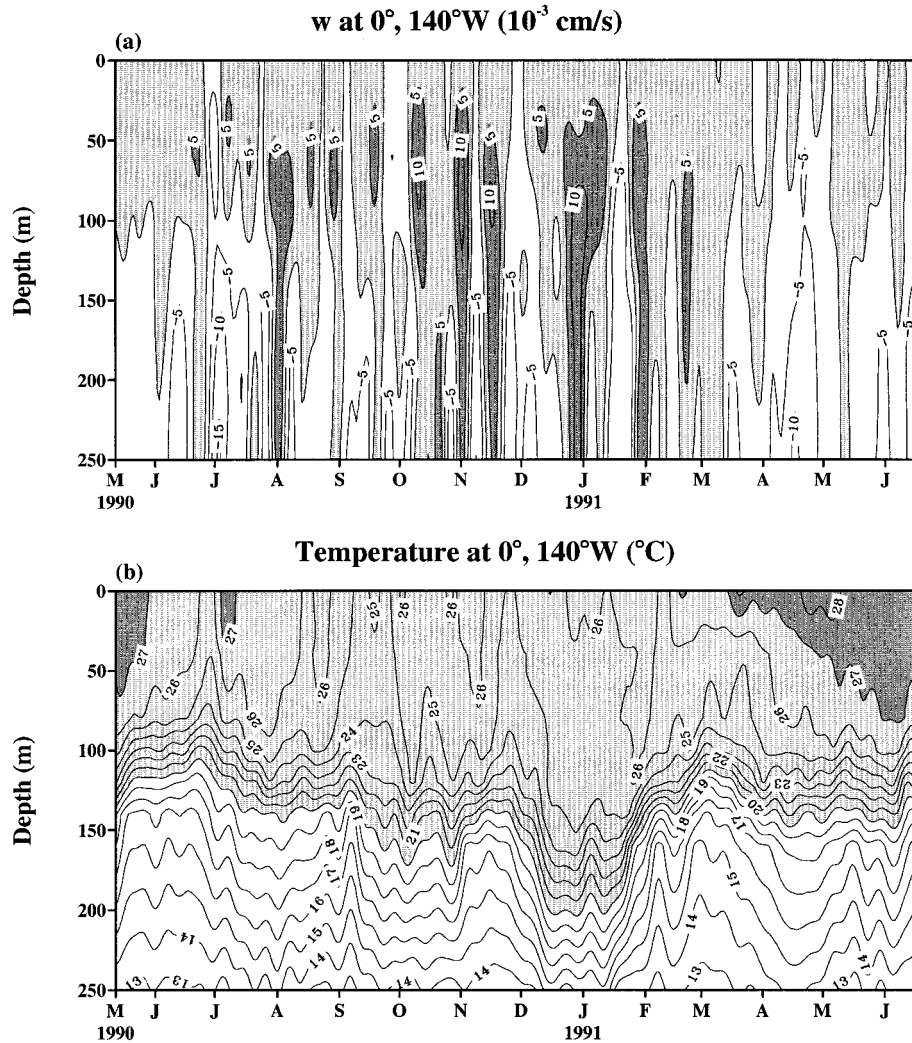
Figure 2. (a) Estimated vertical velocity component from the TIWE array and (b) temperature from the TAO array as functions of time and depth at 0°, 140°W. For vertical velocity, shading denotes upwelling, with dark shading denoting values in excess of 5×10^{-3} cm s^{-1}, and the contour interval is 5×10^{-3} cm s^{-1}. For temperature, shading denotes values larger than 20°C, with dark shading denoting values in excess of 27°C, and the contour interval is 1°C. All data were low-pass filtered to remove oscillations on timescales shorter than 10 days.

the equatorial central Pacific. Note that the increase in SST precedes the reversal in the zonal flow direction, suggesting that the SST is responding to the decrease in upwelling. The instability wave season, which is identified by fairly regular, 3-week oscillations in the v component, includes the period from August through December 1990. (The tropical instability waves, owing their existence to velocity shear [*Philander*, 1978], oscillate with a periodicity of ~3 weeks and have a westward phase speed.) Along with these seasons and transitions, there are several periods during which the isotherms undergo large displacements that are coincident with downwelling or upwelling events. The downwelling events are easier to discern because downwelling tends to be largest where the vertical temperature gradient is large, as contrasted with the upwelling events that tend to be largest within the mixed layer. For instance, note the downwelling events that occur during July/August, September, and November/December 1990 and April/May 1991. The isotherms respond in all of these cases, and during the spring 1991 case, in particular, SST rises rapidly with the decrease in upwelling near the surface and the increase in downwelling below the surface. This relationship

suggests that both upwelling and downwelling are important for SST variations in the equatorial central Pacific.

3. Ocean Circulation Influence on SST

TIWE did not provide direct observation of surface heat flux, so our analysis is limited to the ocean circulation influences on SST. Considering adiabatic processes only, the near-surface temperature will vary in response to the temperature flux divergence according to

$$\frac{\partial T}{\partial t} = - \frac{\partial (uT)}{\partial x} - \frac{\partial (vT)}{\partial y} - \frac{\partial (wT)}{\partial z}, \quad (2)$$

where T is temperature and t is time. The terms in (2) are the local rate of change of temperature and the zonal, meridional, and vertical temperature flux divergences. Combining (2) with the continuity equation (1), the temperature equation may be alternatively written in an advective form:

$$\frac{\partial T}{\partial t} = -u \frac{\partial T}{\partial x} - v \frac{\partial T}{\partial y} - w \frac{\partial T}{\partial z}. \quad (3)$$
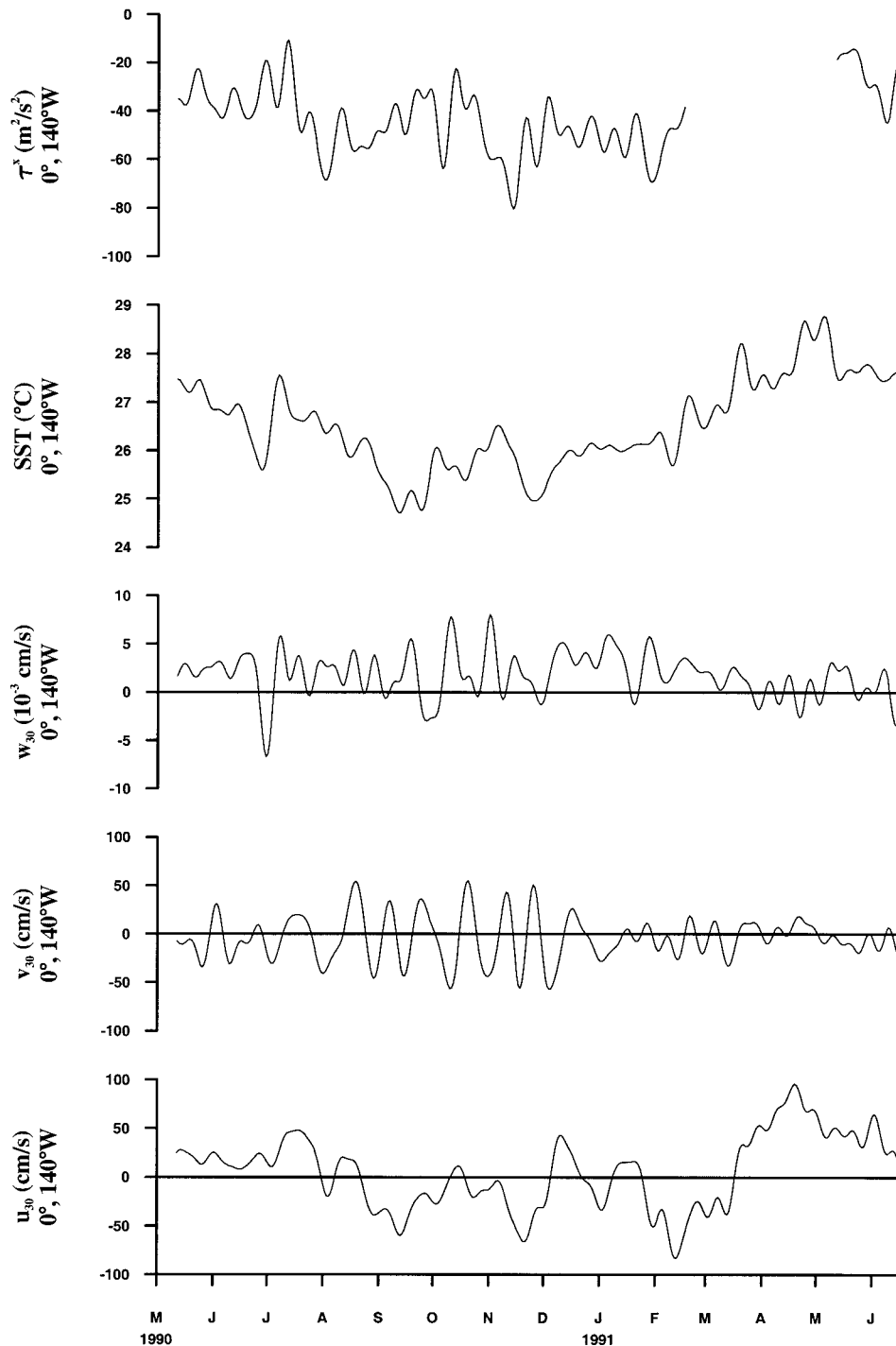
Figure 3. Time series of the zonal wind stress component and SST from the TAO array and the vertical, meridional, and zonal velocity components at 30 m depth from the TIWE array. All time series were low-pass filtered to remove oscillations on timescales shorter than 10 days.

The terms in the right-hand side of (3) are the zonal, meridional, and vertical temperature advections, respectively. Equations (2) and (3) are diagnosed using the TIWE velocity data in combination with the blended SST product for horizontal derivatives and the TAO temperature data for vertical derivatives.

In differential form the flux divergence formulation of (2) is equal to the advective formulation of (3) via the continuity equation (1), but in reality, we have to evaluate these by finite differences. Here we use centered differences to estimate (2)

and (3). In the estimation of (2) we use the u and T data at the TIW3 and TIW1 positions for calculating $\partial(uT)/\partial x$, the v and T data at the TIW5 and TIW2 positions for calculating $\partial(vT)/\partial y$, and the w and T data at the TIW4 position (both w and T are at 20 and 40 m) for calculating $\partial(wT)/\partial z$. In the estimation of (3) we use the u data at the TIW4 position and the T data at the TIW3 and TIW1 positions for calculating $u(\partial T/\partial x)$, the v data at the TIW4 position and the T data at the TIW5 and TIW2 positions for calculating $v(\partial T/\partial y)$, and the w and T data at the TIW4 position (w at 30 m and T at 20 and
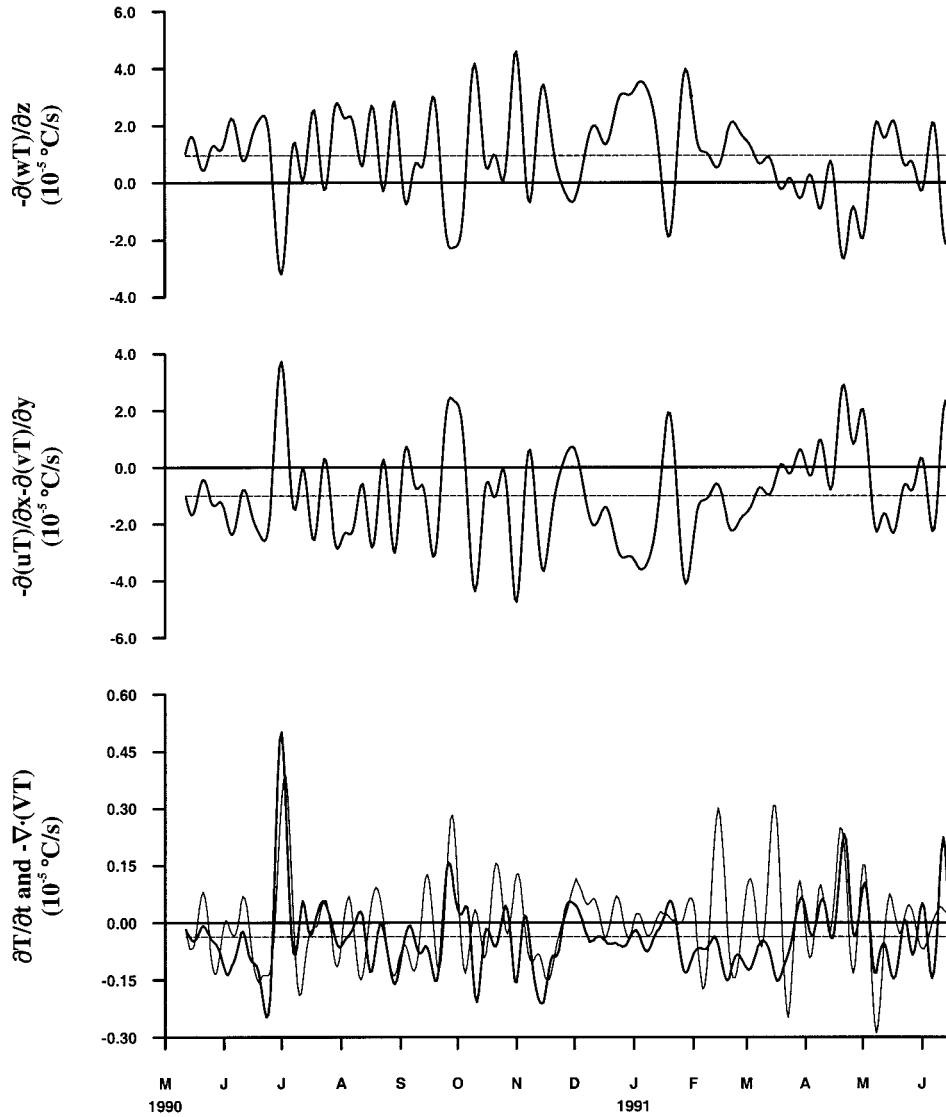
Figure 4. Time series of (a) vertical, (b) horizontal, and (c) total (sum of the vertical and the horizontal) temperature flux divergences calculated at 30 m depth. Superimposed upon the total temperature flux divergence is the observed local rate of change of SST from the TAO mooring (thin curve). Thin horizontal lines are the respective record length mean values of the temperature flux divergence terms. All time series were low-pass filtered to remove oscillations on timescales shorter than 10 days.

40 m) for calculating $w(\partial T/\partial z)$. As shown in Appendix A, the estimates by the flux divergence and advective formulations are equivalent if the following relationships in the observed data hold:

$$u_4 = (u_3 + u_1)/2, \qquad (4)$$

$$v_4 = (v_5 + v_2)/2, \qquad (5)$$

$$w_4 = (w_{up} + w_{low})/2, \qquad (6)$$

$$(T_3 + T_1)/2 = (T_5 + T_2)/2 = (T_{up} + T_{low})/2, \qquad (7)$$

where the subscripts 1, 2, 3, 4, and 5 refer to the TIW1, TIW2, TIW3, TIW4, and TIW5 positions, respectively, as shown in Figure 1, and the subscripts up and low refer to the locations above and below, respectively, the depth at which the vertical temperature advections are estimated. Since these relationships do not exactly hold, the estimations by both formulations are not exactly the same. However, they do provide similar results.

Consider the flux divergence formulation of (2) first. Each term is calculated using a centered difference scheme. The blended SST product, consisting of 1° latitude by 1° longitude averages centered upon every 0.5° of latitude or longitude, is further averaged over four adjacent boxes to provide estimates coincident with the TIWE mooring positions. The diagnostic calculation is performed at 30 m depth since that is the shallowest depth at which we have actual horizontal velocity measurements. The horizontal derivatives are thus calculated using u at the TIW3 and TIW1 positions and v at the TIW5 and TIW2 positions, along with the four-box-averaged blended SST product. The vertical derivative is also calculated at 30 m depth using w estimated from the TIWE array and temperature data from the TAO mooring at the depths of 20 and 40 m. The results are shown in Figure 4a, 4b, and 4c for vertical, horizontal, and total (sum of the vertical and horizontal), temperature flux divergences, respectively. Superimposed upon the total temperature flux divergence is the observed local rate
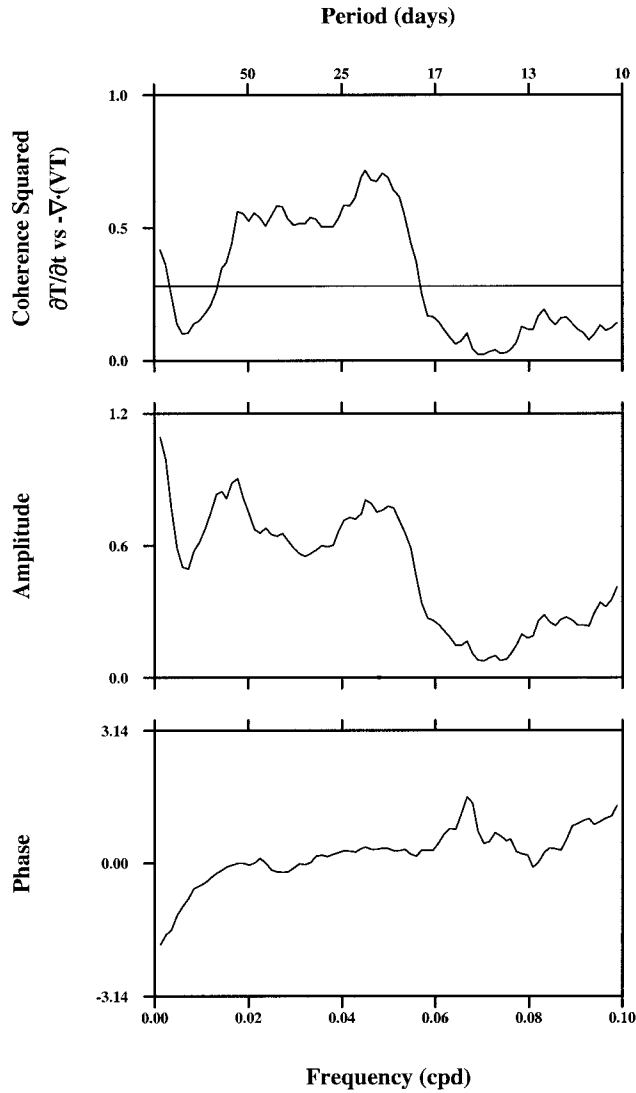
Figure 5. Coherence analysis between the local rate of change of SST ($\partial T/\partial t$) and the total temperature flux divergence $[-\nabla \cdot (vT)]$ showing coherence squared, transfer function amplitude, and phase. Frequency band averaging was performed over a 0.02-cpd bandwidth for ~16 degrees of freedom, and the 90% significance level for the null hypothesis of coherence squared is indicated by the horizontal line.

of change of SST from the TAO mooring (thin curve). The thin horizontal lines represent the record length mean values for the vertical, horizontal, and total temperature flux divergences. The vertical and horizontal terms, calculated independently, are observed to vary out of phase. Internal energy diverging horizontally is counteracted by internal energy converging vertically, with the residual (note the change of scale in Figure 4c panel) determining the ocean circulation's influence on the local rate of change of temperature. The fact that the horizontal and vertical terms look so similar (with opposite sign) is merely a consequence of incompressibility. On average, internal energy is horizontally divergent and vertically convergent, with the divergent water being warmer than the convergent water. Consequently, the net effect of ocean circulation on the equator in the central Pacific is a decrease in internal energy and hence a cooling as seen in Figure 4c.

A corollary to this finding (that ocean circulation, on aver-

age, provides a cooling effect in the equatorial central Pacific) is that a positive net surface heat flux must exist, on average, to balance the cooling effect of ocean dynamics. The record length average total temperature flux divergence $[-\nabla \cdot (\mathbf{v}T)]$ in Figure 4 is -0.037×10^{-5} °C s^{-1}. We may ask if this is consistent with the available net surface heat flux climatologies in this region. Given that the record length average local rate of change of SST is nearly zero and using a control volume depth $h = 30$ m, the equivalent absorbed heat flux is about $\rho C_p h \nabla \cdot (\mathbf{v}T) = 44.4$ W m^{-2}, where $\rho C_p = 4 \times 10^6$ J m^{-3} °C^{-1}. Allowing for a penetrative heat flux past 30 m amounting to ~35 W m^{-2} (estimated using the method of *Hayes et al.* [1991]), the corresponding net surface heat flux is ~79.4 W m^{-2}, which is within the range of the annual mean net surface heat flux in the equatorial central Pacific as given by *Esbensen and Kushnir* [1981], *Oberhuber* [1988], and *Philander et al.* [1987]. It is worth noting that the temperature flux divergence estimated dynamically herein is calculated independently from the thermodynamical heat fluxes of the previous studies, but the results are consistent. Our result is also consistent with the calculation of *Weisberg and Qiao* [2000], who obtained a net upward entrainment of relatively cold water between the EUC core and the surface amounting to ~80 W m^{-2}. The result here is also consistent with the diagnostic box models of *Wyrtki* [1981] and *Bryden and Brady* [1985].

Hansen and Paul [1984] and *Bryden and Brady* [1989] estimated the contributions of the eddy temperature flux to the equatorial Pacific heat budget as *Weisberg and Weingartner* [1988] did for the equatorial Atlantic. We provide similar analyses by decomposing the velocity and temperature fields into mean and fluctuating components:

$$\begin{aligned} u &= \bar{u} + u', \\ v &= \bar{v} + v', \\ w &= \bar{w} + w', \\ T &= \bar{T} + T', \end{aligned} \tag{8}$$

where the overbar denotes the record length mean and the prime denotes fluctuations about the record length mean. The record length mean total temperature flux divergence can then be broken into mean and eddy temperature flux divergences:

$$-\nabla \cdot \overline{\mathbf{v}T} = -\frac{\partial(\bar{u}\,\bar{T})}{\partial x} - \frac{\partial(\bar{v}\,\bar{T})}{\partial y} - \frac{\partial(\bar{w}\,\bar{T})}{\partial z} - \frac{\partial \overline{u'T'}}{\partial x} - \frac{\partial \overline{v'T'}}{\partial y}$$

$$- \frac{\partial \overline{w'T'}}{\partial z}. \tag{9}$$

Our calculations show that $-\partial(\bar{u}\,\bar{T})/\partial x$, $-\partial(\bar{v}\,\bar{T})/\partial y$, and $-\partial(\bar{w}\,\bar{T})/\partial z$ are -0.310×10^{-5} °C s^{-1}, -0.691×10^{-5} °C s^{-1}, and 0.952×10^{-5} °C s^{-1}, respectively, with a net mean temperature flux $(-\nabla \cdot \overline{\mathbf{v}}\,\overline{T})$ of -0.049×10^{-5} °C s^{-1}. The divergences $-\partial(\overline{u'T'})/\partial x$, $-\partial(\overline{v'T'})/\partial y$, and $-\partial(\overline{w'T'})/\partial z$ are -0.0090×10^{-5} °C s^{-1}, 0.0174×10^{-5} °C s^{-1}, and 0.0026×10^{-5} °C s^{-1}, respectively, with a net eddy temperature flux $(-\nabla \cdot \overline{\mathbf{v}'T'})$ of 0.011×10^{-5} °C s^{-1}. From these terms and their sums we find the following: First, $-\nabla \cdot (\overline{\mathbf{v}}\,\overline{T})$ and $-\nabla \cdot (\overline{\mathbf{v}'T'})$ have opposite sign, with the divergence of the net mean temperature flux providing a cooling influence and the convergence of the net eddy temperature flux providing a warming influence. Since the net mean flux divergence exceeds the net eddy flux convergence, the overall effect of the circulation is a cooling influence. Second, cooling occurs for the mean flux since the horizontal mean flux divergence exceeds
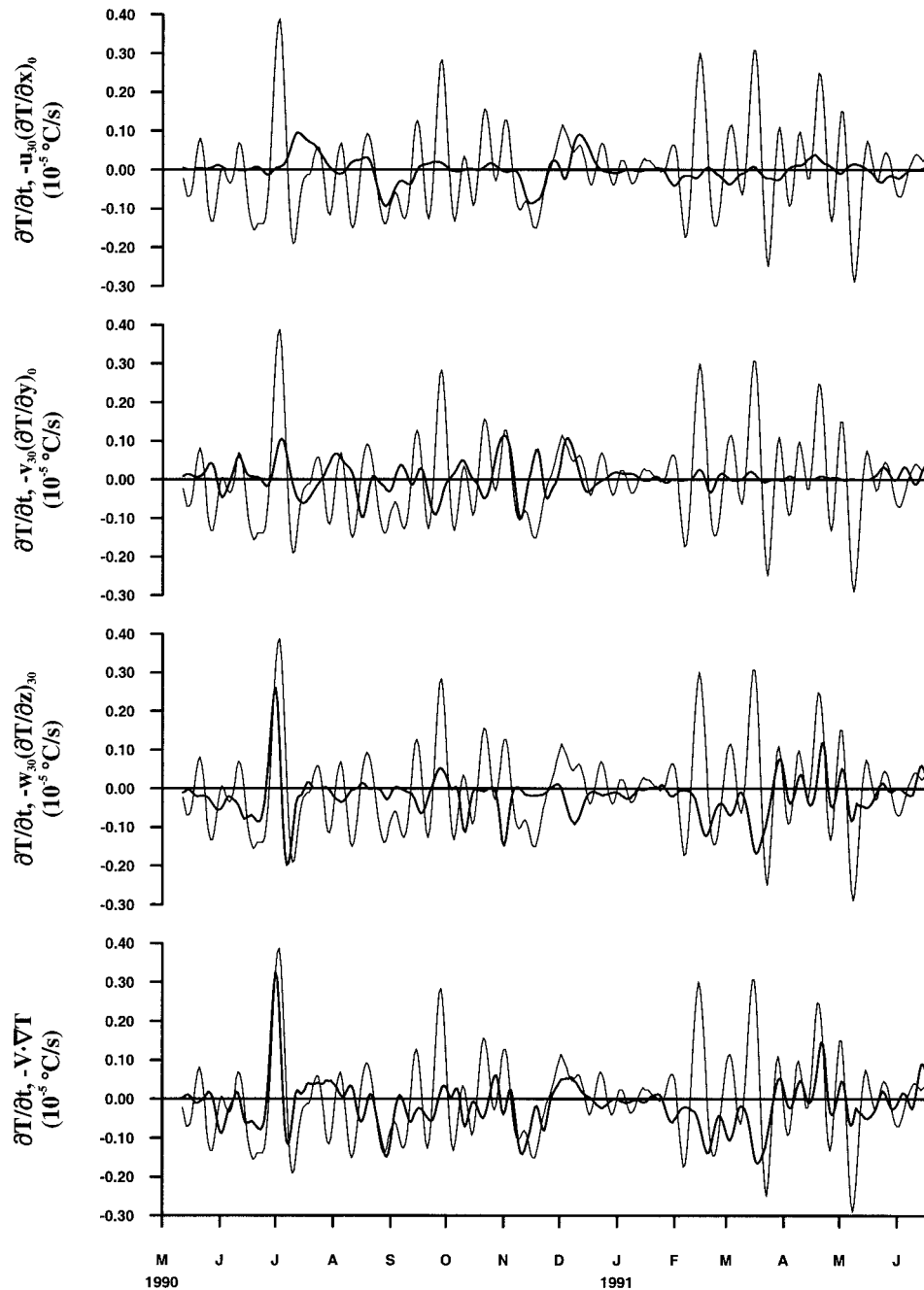
Figure 6. Time series of (top to bottom) zonal, meridional, and vertical temperature advections and their sum calculated at 30 m depth. Superimposed upon each component and their sum is the observed local rate of change of SST (thin curves) from the TAO mooring. All time series were low-pass filtered to remove oscillations on timescales shorter than 10 days.

the vertical mean flux convergence. Hence more internal energy exits the control volume at the sides than external energy enters into the control volume from below. Third, the principal eddy flux term is meridional warming. This is offset somewhat, but not entirely, by zonal cooling. Fourth, unlike the mean terms where the horizontal and vertical flux divergences are of opposite sign, both the horizontal and vertical eddy flux divergences provide warming, on average, to offset cooling by the mean temperature flux divergence.

A visual comparison of the fluctuations in $-\nabla \cdot (\mathbf{v}T)$ versus $\partial T/\partial t$ in Figure 4 shows that there are intervals when these

time series covary in unison with nearly corresponding amplitudes and intervals when they do not. Particularly noticeable downwelling and warming events occur during the beginning of July, October, and December 1990 and during the entire month of April 1991. These downwelling events correspond with some of the largest increases in SST, as seen in Figure 3. Similarly noticeable upwelling and cooling events occur during the end of June, August, and the middle of November 1990, again corresponding with some of the largest decreases in SST. Interestingly, the largest upwelling event observed in Figure 2 had a negligible effect on SST because the thermocline was

Period (days)
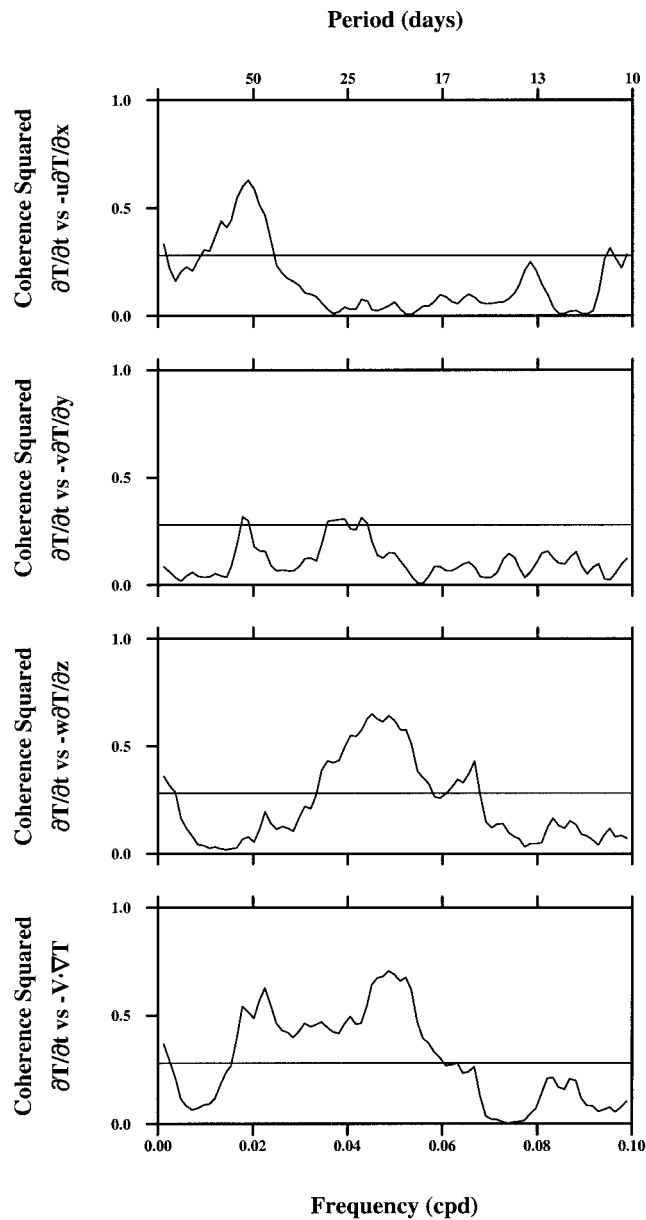
Frequency (cpd)

Figure 7. Coherence analysis between local rate of change of SST ($\partial T/\partial t$) and (top to bottom) zonal, meridional, and vertical temperature advections and their sum. Frequency band averaging was performed over a 0.02-cpd bandwidth for ~16 degrees of freedom, and the 90% significance level for the null hypothesis of coherence squared is indicated by the horizontal lines.

relatively deep and the vertical temperature gradient was correspondingly small. Thus, despite a sustained period of upwelling from mid-December to January, SST remained relatively constant. This visual comparison may be quantified through a coherence analysis as shown in Figure 5. Within a bandwidth including timescales of roughly 2.5 weeks to 2.5 months (encompassing the instability waves through the intraseasonal oscillations), ~50–60% of SST variation is accounted for by ocean circulation variability. Given that the calculations are based on a combination of different data sets (the TIWE velocity, TAO temperature, and blended SST) with

different spatial and temporal scales, the results are surprisingly good.

The results using the advective formulation of (3) are shown in Figure 6 for (top to bottom) zonal advection, meridional advection, vertical advection, and their sum, all superimposed upon the observed local rate of change of SST from the TAO mooring (thin curves). The ocean circulation effects upon SST are fully 3-D, with the vertical advection being the most important and the zonal advection being the least important of the three terms. Neither the zonal advection nor the meridional advection has a record length average that is appreciably different from zero. It is only during the instability wave season that the meridional advection shows appreciable fluctuations, but even then, the average meridional temperature advection is not appreciably different from zero. There are only two occasions in the entire record when the zonal advection appears to provide the major influence on SST. These correspond to the peaks during September and November 1990 in the surface westward flowing South Equatorial Current. At other times, zonal advection effects are offset by either or both of the other two velocity components. Meridional advection effects are only noticeable during the instability wave season. During this interval they tend to oppose the effects of vertical advection, as has been noted in numerical models of the tropical Atlantic and Pacific Oceans [e.g., *Philander et al.*, 1986] and in observations of the equatorial Atlantic Ocean [*Weingartner and Weisberg*, 1991a].

A coherence analysis between the local rate of change of SST and the different SST advection terms (Figure 7) helps to clarify the various timescales within which the effects of these terms are manifest. The coherence squared between the local rate of change of SST and the zonal advection is nearly zero, except around a narrow band located at intraseasonal timescales. For the meridional advection, marginal coherence exists at both intraseasonal and instability wave timescales. The vertical advection shows the largest coherence with the local rate of change of SST on timescales bracketing the instability waves. Summing the effects of the fully 3-D advection results in a very similar coherence distribution to that shown in Figure 5.

The moored measurements around 0°, 140°W do not allow us to calculate the net surface heat flux. However, latent and sensible heat fluxes can be estimated from the TAO moored data using bulk formulas. The sum of latent and sensible heat fluxes (Q) at 0°, 140°W, along with the surface wind speed and the SST from which they derive, are shown in Figure 8. The variations in Q (primarily latent heat flux from the ocean to the atmosphere) are large, with peaks in Q tending to correspond with SST minima and troughs in Q tending to correspond with SST maxima. As seen in Figure 9, Q is coherent with SST over the timescales of the tropical instability waves. The relationship is not a directly causal one, however, because Q and SST are observed to be in phase as opposed to being in quadrature (a 90° phase lag between SST and Q). The relationship between SST and Q observed within the instability wave band can be explained as follows. The local SST perturbations associated with the tropical instability waves affect the local winds by modifying the atmospheric boundary layer. When cold air passes over relatively warm water, the atmospheric boundary layer is destabilized [*Hayes et al.*, 1989], resulting in reduced wind shear and increased wind speed near the sea surface. Since latent and sensible heat fluxes are primarily determined by surface wind speed [e.g., *Liu et al.*, 1994; *Zhang and McPhaden*, 1995; *Wang*, 1995; *Weisberg and Wang*, 1997], this ac-
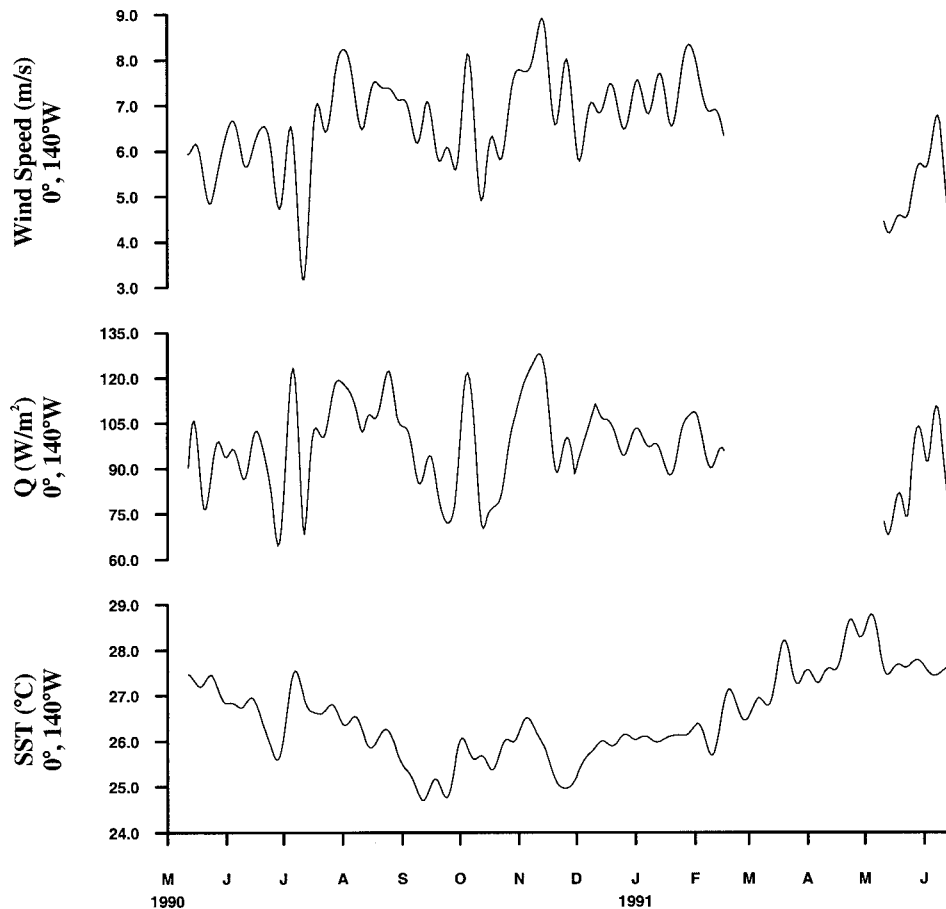
Figure 8. Time series of (top) surface wind speed, (middle) sum of latent and sensible heat fluxes (Q), and (bottom) SST. All time series were low-pass filtered to remove oscillations on timescales shorter than 10 days.

counts for the observed coherence and phase between the SST and Q within the instability wave band.

4. Summary and Discussion

Horizontal velocity data from a five element array of moored ADCPs deployed about 0°, 140°W from May 1990 to June 1991 during the TIWE, combined with TAO array data and a blended SST product, were used to study ocean circulation effects upon SST in the equatorial central Pacific. The TIWE horizontal velocity data allowed us to calculate the vertical velocity component by vertically integrating the continuity equation and by using centered differences for the horizontal divergence. The ocean temperature equation was diagnosed using both flux divergence and advective formulations. The effects of the ocean circulation upon SST were found to be fully 3-D, with the vertical component being the most important and the zonal component being the least important contributor. Upwelling and downwelling were found to be associated with cooling and warming, respectively. This suggests that downwelling should also be considered in parameterizations of vertical velocity effects on model SST (some intermediate models assume that downwelling does not affect SST). Quantitatively, ~50–60% of the observed SST variation on timescales longer than 10 days was accounted for by the ocean circulation. The results are encouraging, given that the TIWE equatorial array did not have concomitant temperature mea-

surements, which forced us to use a weekly SST product that barely resolves the instability waves. The results suggest that with velocity and temperature data sampled on the same spatial and temporal scales, ocean circulation effects on SST may become better defined. A complete moored array that measures all of the physical processes controlling SST variations (including surface heat flux) is needed in future field experimentation.

Nonadiabatic effects must also be considered. On average, the ocean circulation provides a cooling effect, and this cooling, resulting from ocean dynamics, must be balanced by a net surface heat flux. Considering the record length average convergence of heat flux by ocean circulation that was estimated within an upper ocean 30-m control volume and providing for penetrative radiation beyond 30 m depth, our result for net surface heat flux of ~80 W m^{-2} is quantitatively consistent with existing climatological mean estimates of surface heat flux [e.g., *Esbensen and Kushnir*, 1981; *Oberhuber*, 1988]. The result is also consistent with other studies [e.g., *Wyrtki*, 1981; *Bryden and Brady*, 1985; *Philander et al.*, 1987; *Weisberg and Qiao*, 2000]. Surface heat flux on intraseasonal, instability wave, and other timescales is also important. While moored data are not sufficient for a rigorous temperature budget analysis, latent and sensible heat flux estimates by bulk formulas show that a direct causal relationship between these heat flux constituents and SST does not exist. Instead, as shown by *Hayes et al.* [1989],

Period (days)
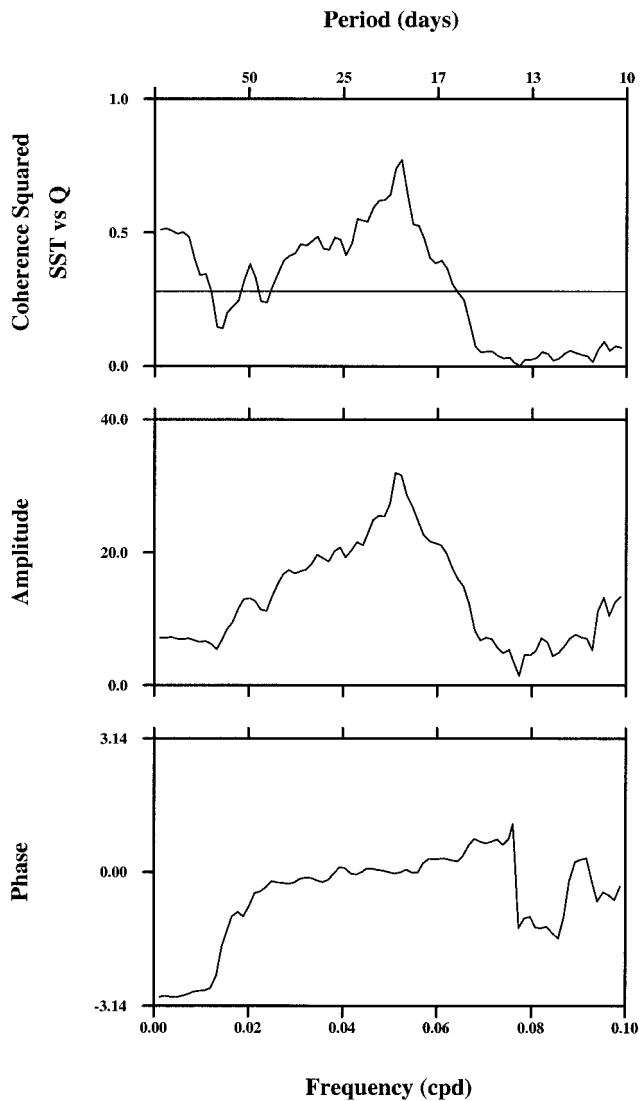
Figure 9. Coherence analysis between SST and sum of latent and sensible heat fluxes (Q) showing coherence squared, transfer function amplitude, and phase. Frequency band averaging was performed over a 0.02-cpd bandwidth for ~16 degrees of freedom, and the 90% significance level for the null hypothesis of coherence squared is indicated by the horizontal line.

the SST variations associated with instability waves appear to modify the winds and hence the fluxes.

Previous microstructure investigations showed that turbulent vertical heat flux may make significant contributions to the equatorial heat budget within the ocean mixed layer [e.g., *Peters et al.*, 1988; *Moum et al.*, 1989; *Lien et al.*, 1995]. In section 3 we break the record length mean total temperature flux divergence into the mean and eddy temperature flux divergences (see (9)) and estimate the individual terms. The vertical eddy flux divergence of $-\partial(\overline{w'T'})/\partial z$ does contribute to the mean total temperature flux divergence. However, since the data are low-pass filtered for use with the weekly blended SST product, our calculations may exclude the part of turbulent contribution on shorter timescales.

Using an ocean general circulation model, *Koberle and Philander* [1994] investigated the seasonal variations of SST in the

tropical Pacific. They showed that in the equatorial eastern Pacific, there is a positive net surface heat flux into the ocean at practically all times, but temperature nonetheless decreases between April and September. This cooling is caused by temperature advection, primarily in the vertical direction [*Koberle and Philander*, 1994, Figure 11]. Their results are supported by the observations reported herein.

Using drifter and current meter data, respectively, *Hansen and Paul* [1984] and *Bryden and Brady* [1989] showed a substantial eddy heat flux convergence in the equatorial Pacific. The calculations herein based on the TIWE data are consistent with these studies in that the meridional eddy temperature flux is convergent. Our calculations also showed that the vertical and zonal eddy temperature fluxes are much smaller than the meridional eddy temperature flux. Despite the eddy meridional heat flux convergence, eddy heat flux plays a secondary role in the equatorial heat budget. The heat flux in the equatorial central Pacific is dominated by mean heat flux. The cooling effect of the ocean circulation observed in the equatorial central Pacific is mainly controlled by mean circulation and temperature fields.

The variation of the equatorial cold tongue will change the zonal SST gradients of the tropical Pacific. These gradients in turn determine the large-scale tropical ocean-atmosphere interactions and hence global climate variations [*Bjerknes*, 1966, 1969]. It follows that independently determining the physical processes controlling cold tongue SST variations by field experimentation is a necessary step toward improving climate prediction by numerical models. Since the TIWE did not include temperature and air-sea interaction measurements (such as the Improved Meteorology Sensor System (IMET) instruments for air-sea fluxes [*Weller and Anderson*, 1996]), the analyses presented herein had to rely on a combination of the TIWE velocity data, the TAO array temperature and wind data, and a blended SST product. While our results are encouraging, the data mismatch in both spatial and temporal scales may have biased the calculation of the ocean circulation's influence on SST. Ideally, an experimental study on the relative importances of the processes controlling the cold tongue SST variations should resolve the scales of the relevant ocean and atmosphere contributions to the temperature equation. Since a flux divergence formulation appears to perform better than an advective formulation, future field work should employ a TIWE-like array including temperature, salinity, and air-sea interaction measurements to better define the dynamical and thermodynamical influences on cold tongue SST.

Appendix A: Comparison of Temperature Advective and Flux Divergence Finite Difference Formulations

In differential form the temperature flux divergence formulation of (2) and the temperature advective formulation of (3) are equivalent via the continuity equation (1). Since these two formulations are calculated in the finite difference schemes using the moored data, we examine how they differ and at what conditions they are equivalent.

The finite centered differences for the individual terms in the advective formulation are

$$u \frac{\partial T}{\partial x} \approx u \frac{\Delta T}{\Delta x} = u_4 \frac{T_3 - T_1}{x_3 - x_1}, \qquad (A1)$$

$$v \frac{\partial T}{\partial y} \approx v \frac{\Delta T}{\Delta y} = v_4 \frac{T_5 - T_2}{y_5 - y_2}, \qquad (A2)$$

$$w \frac{\partial T}{\partial z} \approx w \frac{\Delta T}{\Delta z} = w_4 \frac{T_{\text{up}} - T_{\text{low}}}{z_{\text{up}} - z_{\text{low}}}, \qquad (A3)$$

where the subscripts 1, 2, 3, 4, and 5 refer to the TIW1, TIW2, TIW3, TIW4, and TIW5 positions, respectively, as shown in Figure 1, and the subscripts up and low refer to the locations above and below, respectively, the depth at which the vertical temperature advections are estimated. The finite centered differences for the individual divergence terms in the flux divergence formulation are

$$\frac{\partial(uT)}{\partial x} \approx \frac{\Delta(uT)}{\Delta x} = \frac{(u_3 T_3 - u_1 T_1)}{x_3 - x_1} = \frac{(u_3 + u_1)}{2} \frac{(T_3 - T_1)}{x_3 - x_1}$$

$$+ \frac{(T_3 + T_1)}{2} \frac{(u_3 - u_1)}{x_3 - x_1}, \qquad (A4)$$

$$\frac{\partial(vT)}{\partial y} \approx \frac{\Delta(vT)}{\Delta y} = \frac{(v_5 T_5 - v_2 T_2)}{y_5 - y_2} = \frac{(v_5 + v_2)}{2} \frac{(T_5 - T_2)}{y_5 - y_2}$$

$$+ \frac{(T_5 + T_2)}{2} \frac{v_5 - v_2}{y_5 - y_2}, \qquad (A5)$$

$$\frac{\partial(wT)}{\partial z} \approx \frac{\Delta(wT)}{\Delta z} = \frac{(w_{\text{up}} T_{\text{up}} - w_{\text{low}} T_{\text{low}})}{z_{\text{up}} - z_{\text{low}}}$$

$$= \frac{(w_{\text{up}} + w_{\text{low}})}{2} \frac{(T_{\text{up}} - T_{\text{low}})}{z_{\text{up}} - z_{\text{low}}}$$

$$+ \frac{(T_{\text{up}} + T_{\text{low}})}{2} \frac{(w_{\text{up}} - w_{\text{low}})}{z_{\text{up}} - z_{\text{low}}}. \qquad (A6)$$

If the following relationships hold:

$$u_4 = (u_3 + u_1)/2, \qquad (A7)$$

$$v_4 = (v_5 + v_2)/2, \qquad (A8)$$

$$w_4 = (w_{\text{up}} + w_{\text{low}})/2, \qquad (A9)$$

$$\frac{(T_3 + T_1)}{2} = \frac{(T_5 + T_2)}{2} = \frac{(T_{\text{up}} + T_{\text{low}})}{2} \equiv T_4, \qquad (A10)$$

then we have

$$\frac{\partial(uT)}{\partial x} + \frac{\partial(vT)}{\partial y} + \frac{\partial(wT)}{\partial z} \approx \frac{\Delta(uT)}{\Delta x} + \frac{\Delta(vT)}{\Delta y} + \frac{\Delta(wT)}{\Delta z}$$

$$= u_4 \frac{(T_3 - T_1)}{x_3 - x_1} + v_4 \frac{(T_5 - T_2)}{y_5 - y_2} + w_4 \frac{(T_{\text{up}} - T_{\text{low}})}{z_{\text{up}} - z_{\text{low}}}$$

$$+ T_4 \left(\frac{u_3 - u_1}{x_3 - x_1} + \frac{v_5 - v_2}{y_5 - y_2} + \frac{w_{\text{up}} - w_{\text{low}}}{z_{\text{up}} - z_{\text{low}}} \right)$$

$$= u \frac{\Delta T}{\Delta x} + v \frac{\Delta T}{\Delta y} + w \frac{\Delta T}{\Delta z}. \qquad (A11)$$

In the derivation of (A11) we have used the finite difference form of the continuity equation (1). Therefore the temperature advective finite difference formulation and the temperature flux divergence finite difference formulation are equivalent if the relationships of (A7)–(A10) in observed data are true.

References

Bjerknes, J., A possible response of the atmospheric Hadley circulation to equatorial anomalies of ocean temperature, *Tellus*, *18*, 820–829, 1966.

Bjerknes, J., Atmospheric teleconnections from the equatorial Pacific, *Mon. Weather Rev.*, *97*, 163–172, 1969.

Bryden, H. L., and E. C. Brady, Diagnostic model of three-dimensional circulation in the upper equatorial Pacific Ocean, *J. Phys. Oceanogr.*, *5*, 1255–1273, 1985.

Bryden, H. L., and E. C. Brady, Eddy momentum and heat fluxes and their effects on the circulation of the equatorial Pacific Ocean, *J. Mar. Res.*, *47*, 55–79, 1989.

Esbensen, S. K., and V. Kushnir, The heat budget of the global ocean: An atlas based on estimates from surface marine observations, *Rep. 29*, 27 pp. and 188 figures, Clim. Res. Inst., Oreg. State Univ., Corvallis, 1981.

Halpern, D., and P. H. Freitag, Vertical motion in the upper ocean of the equatorial eastern Pacific, *Oceanol. Acta*, *Spec. Vol. 6*, 19–26, 1987.

Halpern, D., R. A. Knox, D. S. Luther, and S. G. H. Philander, Estimates of equatorial upwelling between 140°W and 110°W during 1984, *J. Geophys. Res.*, *94*, 8018–8020, 1989.

Hansen, D., and C. Paul, Genesis and effects of long waves in the equatorial Pacific, *J. Geophys. Res*, *89*, 10,431–10,440, 1984.

Hayes, S. P., M. McPhaden, and J. M. Wallace, The influence of sea surface temperature on surface wind in the eastern equatorial Pacific: Weekly to monthly variability, *J. Clim.*, *2*, 1500–1506, 1989.

Hayes, S. P., P. Chang, and M. McPhaden, Variability of the sea surface temperature in the eastern equatorial Pacific during 1986–1988, *J. Geophys. Res.*, *96*, 10,553–10,566, 1991.

Kessler, W. S., and M. J. McPhaden, The 1991–1993 El Niño in the central Pacific, *Deep Sea Res.*, *Part II*, *42*, 295–333, 1995.

Koberle, C., and S. G. Philander, On the processes that control seasonal variations of sea surface temperature in the tropical Pacific Ocean, *Tellus*, *Ser. A*, *46*, 481–496, 1994.

Lien, R. C., D. R. Caldwell, M. C. Gregg, and J. N. Moum, Turbulence variability at the equator in the central Pacific at the beginning of the 1991–1993 El Niño, *J. Geophys. Res.*, *100*, 6881–6898, 1995.

Liu, W. T., A. Zhang, and J. K. B. Bishop, Evaporation and solar irradiance as regulators of sea surface temperature in annual and interannual changes, *J. Geophys. Res.*, *99*, 12,623–12,637, 1994.

McPhaden, M. J., TOGA-TAO and the 1991–93 El Niño–Southern Oscillation event, *Oceanography*, *6*, 36–44, 1993.

Moum, J. N., D. R. Caldwell, and C. A. Paulson, Mixing in the equatorial surface layer and thermocline, *J. Geophys. Res.*, *94*, 2005–2021, 1989.

Oberhuber, J. M., An atlas based on the COADS data set: The budget of heat, buoyancy and turbulent kinetic energy at the surface of the global ocean, *Rep. 15*, 199 pp., Max-Planck-Inst. für Meteorol., Hamburg, Germany, 1988.

Peters, H., M. C. Gregg, and J. M. Toole, On the parameterization of equatorial turbulence, *J. Geophys. Res.*, *93*, 1199–1218, 1988.

Philander, S. G. H., Instabilities of zonal equatorial currents, *J. Geophys. Res.*, *83*, 3679–3682, 1978.

Philander, S. G. H., W. J. Hurlin, and R. C. Pacanowski, Properties of long equatorial waves in models of the seasonal cycle in tropical Atlantic and Pacific Oceans, *J. Geophys. Res.*, *91*, 14,207–14,211, 1986.

Philander, S. G. H., W. J. Hurlin, and A. D. Seigel, Simulation of the seasonal cycle of the tropical Pacific Ocean, *J. Phys. Oceanogr.*, *17*, 1986–2002, 1987.

Qiao, L., and R. H. Weisberg, Tropical instability wave kinematics: Observations from the Tropical Instability Wave Experiment, *J. Geophys. Res.*, *100*, 8677–8693, 1995.

Qiao, L., and R. H. Weisberg, The zonal momentum balance of the Equatorial Undercurrent in the central Pacific, *J. Phys. Oceanogr.*, *27*, 1094–1119, 1997.

Qiao, L., and R. H. Weisberg, Tropical instability wave energetics: Observations from the Tropical Instability Wave Experiment, *J. Phys. Oceanogr.*, *28*, 345–360, 1998.

Reynolds, R. W., and T. M. Smith, A high-resolution global sea surface temperature climatology, *J. Clim.*, *8*, 1571–1583, 1995.

Wang, C., Numerical, analytical, and observational studies of tropical ocean-atmosphere interactions, Ph.D. dissertation, 184 pp., Univ. of South Fla., St. Petersburg, 1995.

Weingartner, T. J., and R. H. Weisberg, On the annual cycle of equatorial upwelling in the central Atlantic Ocean, *J. Phys. Oceanogr.*, *21*, 68–82, 1991a.

Weingartner, T. J., and R. H. Weisberg, A description of the annual cycle in sea surface temperature and upper ocean heat in the equatorial Atlantic, *J. Phys. Oceanogr.*, *21*, 83–96, 1991b.

Weisberg, R. H., and L. Qiao, Equatorial upwelling in the central Pacific estimated from moored velocity profilers, *J. Phys. Oceanogr.*, *30*, 105–124, 2000.

Weisberg, R. H., and C. Wang, Slow variability in the equatorial west-central Pacific in relation to ENSO, *J. Clim.*, *10*, 1998–2017, 1997.

Weisberg, R. H., and T. J. Weingartner, Instability waves in the equatorial Atlantic Ocean, *J. Phys. Oceanogr.*, *18*, 1641–1657, 1988.

Weller, R. A., and S. P. Anderson, Surface meteorology and air-sea fluxes in the western equatorial Pacific warm pool during the TOGA COARE, *J. Clim.*, *9*, 1959–1990, 1996.

Wyrtki, K., An estimate of equatorial upwelling in the Pacific, *J. Phys. Oceanogr.*, *11*, 1205–1214, 1981.

Zhang, G. J., and M. J. McPhaden, The relationship between sea surface temperature and latent heat flux in the equatorial Pacific, *J. Clim.*, *8*, 589–605, 1995.

———————————

C. Wang, NOAA/AOML/PhOD, 4301 Rickenbacker Causeway, Miami, FL 33149, USA. (wang@aoml.noaa.gov)

R. H. Weisberg, College of Marine Science, 140 Seventh Ave. South, St. Petersburg, FL 33701-5016, USA. (weisberg@marine.usf.edu)